Micro-Phase Separation Kinetics of Polyurethane Nanocomposites With Neural Network

Iman Sahebi Jouibari, Vahid Haddadi-Asl, Hanie Ahmadi, Mohammad Masoud Mirhosseini
Department of Polymer Engineering and Color Technology, Amirkabir University of Technology (Tehran Polytechnic), Tehran, Iran

Thermoplastic polyurethane elastomers (TPUs) reinforced with multi wall carbon nanotubes (MWCNTs) and Closite30B, were prepared via melt mixing approach and investigated by spectroscopy, and rheological analyses. Following basic analyses, time sweep tests were used to determine the influence of temperature, applied preshear and nanofiller content and aspect ratio on the micro-phase separation kinetics of the nanocomposites. Based on the experimental results, artificial neural network was developed to explain the relationship between those parameters and micro-phase separation time. The neural network is able to predict micro-phase separation time of TPU nanocomposites possessing different nanofillers at various shear rates and temperatures. Comparison between experimental and calculated data by the model shows that the neural network can well-communicate between input and target variables. POLYM. COMPOS., 2019. © 2019 Society of Plastics Engineers

INTRODUCTION

Thermoplastic polyurethane elastomers (TPUs), among the most useful block copolymer, have been subject of a plethora of researches for numerous years and several studies have been implemented to reveal more complexity of those copolymers. TPUs can be used as elastomer, soft foam, hard foam, pigment, and so forth. The structure and property flexibility of the polyurethanes has made them appropriate for various applications. Micro phase separation in PUs occurs due to the thermodynamic incompatibility of the soft and hard segments. It is well understood that hard segment-rich domains act as physical crosslinks and their outstanding mechanical properties are manifested in TPUs [1–3].

Many factors like polymerization procedures, chemical nature of the hard and soft segments, process parameters (melting rate, cooling rate, shear rate, temperature, etc.) affect the morphology and micro-phase separation of the polyurethanes elastomers [4–6].

Correspondence to: V. Haddadi-Asl; e-mail: haddadi@aut.ac.ir
DOI 10.1002/pc.25250
Published online in Wiley Online Library (wileyonlinelibrary.com).

Due to the extremely high surface area in nanocomposites, an improvement of the mechanical, barrier and thermo-mechanical properties, and conductivity can be achieved at low filler contents (less than 5 wt%) which marks the main advantage of these materials over the microparticle reinforced composites [7–10]. When the effect of nanofillers is studied on the micro-phase separation of TPU nanocomposites, properties of the nanofillers like particle size, aspect ratio, shape, chemical nature and their interaction with polymer should be considered [11, 12]. For example, Barick and Tripathy have shown that the incorporation of the MWCNTs in TPUs matrix accelerates the micro-phase separation of the TPU matrix [13]. Moreover, the crystallinity of the TPU/MWCNT nanocomposites has noticeably increased comparing pristine TPU due to positive nucleating effect of MWCNTs.

Gupta et al. have reported that nucleation effect of the MWCNTs into the polyurethane matrix increases the onset and peak temperatures of crystallization [14].

Song et al. have proposed that the incorporation of nanoclay into the polyurethane decreases the size of the spherical domain, supporting the key role of nanoclay on the aggregation performance of the hard domains [15].

For the investigation of effect of shear flow on phase separation of TPUs, Mourier et al. have studied nano-structuring kinetics of thermoplastic segmented polyurethanes with or without preshear [16, 17]. It has been reported that the time of the structuring kinetics in presheared samples is highly reliant on the composition and type of hard and soft segments. Moreover, preshear treatment reduces the hard domain agglomeration. Consequently, the preshear is found to decrease the entropy of the polymer chains and make them be aligned, thus, promoting the kinetics of phase separation. On the other hand, in the presence of nanofillers, chain dynamics decreases in order to trap the chains onto the nanofiller surfaces and prevent chain orientation. Collectively, the preshear and nanofillers simultaneously affect the micro-phase separation and crystallization of the polyurethanes. Considering the indispensable role of preshear [18, 19] and nanofillers [20, 21] in both laboratory and industrial processes (extrusion, injection molding, etc.) of polyurethane, it would be imperative to study the effect of the previously mentioned parameters on the micro-phase separation of the polyurethanes.

Considering the effect of phase separation on the final properties of TPU, a quantitative relationship between the factors affecting phase separation and phase separation time is necessary. The intelligent artificial neural network (ANN) method is used for modeling because of its high power. ANN is efficient for solving complex problems. This method is used in various fields for example, finding optimal process conditions, estimation of materials properties, fault detection, system identification, and many other subjects [22–25].

Among the available different techniques for simulation, usually ANN is preferred because it is more comprehensive and generally generates better results, even, when the relationship between the input variables and the target variables is nonlinear and intricate. In engineering applications, the feedforward neural network is often used. The most popular type is the multi-layer perceptron (MLP) as it has a high level of training ability [26, 27].

The ANN method is widely used to investigate the characteristics of polymers and polymer nanocomposites. For instance, the permeability of various gases from polyurethane urea has been investigated by Hanna et al. Also, Kupal et al. modeled the Tan (δ) parameter and the viscoelastic behavior of TPU using ANN. The present article aims to quantitatively examine the factors affecting the phase separation behavior of the TPU nanocomposite containing different nanoparticles [25, 28–30].

Hence, the goal of this work was to investigate the effect of temperature, preshear, and nanofillers with different aspect ratios and structures (MWCNTs, Closite 30B) on the micro-phase separation of TPU nanocomposites. To this end, firstly, TPUs were synthesized. Thereafter, TPU nanocomposites were prepared by melt processing and evaluated by Fourier transform infrared (FTIR) spectroscopy and different rheological analyses (RMS), and then the results were classified for ANN in order to better understand the effect of different factors.

MATERIALS AND METHODS

Materials

Poly(tetramethylene ether)glycol (PTMG) with functionality of two and number–average molecular weight of 2000 (g/mol), 4,4′-Diphenylmethane diisocyanate (MDI), 1,4-butanediol (BDO) were purchased from Sigma–Aldrich. The multi-wall carbon nanotubes Nanocyl 7,000 with average diameter of 9.5 nm, average length of 1.5 μm, purity of 90% and aspect ratio of 275 were supplied by Nanocyl (Belgium). Organically modified clay Closite30B (CEC: 90 meq/100 g, $A_f = 10$) was obtained from the southern Clay product. N,N-Dimethylacetamide (DMAC) was obtained from Merck.

Synthesis of TPU

TPU was synthesized by a two-step solution polymerization method. Polymerization was carried out into a two-necked round-bottomed flask equipped with a vacuum inlet tube and a raw material entrance. The reaction assembly was placed in a heating oil bath. Prior to mixing, PTMG, MDI, and BDO were dried in a vacuum oven at 75°C for 3 h to ensure residual moisture removal. For polyurethane synthesis, the molar ratio of PTMG, MDI, and BDO were determined to be 1, 3, and 2, respectively. Thirty grams PTMG with 45 mL DMAC was added to the flask. Later on, 11.6 g MDI was added to the content and reacted with polyol for 3 h at 80°C under continuous stirring to render a macro diisocyanate prepolymer. In the chain extension step, 2.74 g BDO was added to the prepolymer. During this step, the viscosity of polyurethane was slowly increased due to the ongoing chain-extension reaction. After 3 h reaction, the viscous liquid obtained was poured into a silicone mold and placed in an oven at 85°C for 24 h. Finally, all samples were removed from the mold and stored at ambient temperature.

TPU Nanocomposites Preparation

Nanocomposites were prepared via melt compounding method. TPU and varying content of MWNTs (from 0.1 wt% to 2 wt%) and Closite30 B (from 0.15 wt% to 7 wt%) were compounded with a laboratory internal mixer (Braebender Plasticorder W50). Temperature and rotating speed were optimized as 210°C and 100 rpm, respectively. Melt-compounding was performed 12 min for nanocomposites containing the MWNTs and 15 min for Closite30 B. Prior to mixing, TPUs were dried in a vacuum oven at 100°C for 24 h to ensure residual moisture removal. The list of nanocomposite samples is shown in Table 1.

Characterization

FTIR spectra were recorded on a Bruker spectrophotometer within a range of 500–4,400/cm using a resolution of 4/cm. The samples were prepared on a KBr pellet in vacuum desiccators under a pressure of 0.01 Torr.

To measure the linear viscoelastic responses of neat TPU and the nanocomposites, a rheometrics mechanical spectrometer (Paar Physica UDS200) equipped with a parallel plate fixture (25 mm diameter and a constant gap of 1 mm) was employed. The neat TPU and the nanocomposites were heated for 10 min at melting temperature to remove thermal and processing history. The samples were cooled rapidly to the annealing temperature. This cooling

TABLE 1. Compounding formulation Closite 30B and MWCNT samples.

Sample	Closite 30B loading wt%	Sample	MWCNT loading wt%
CB1	0.15	CNT1	0.1
CB2	0.5	CNT2	0.2
CB3	1	CNT3	0.4
CB4	3	CNT4	0.8
CB5	5	CNT5	1.2
CB6	7	CNT6	2

DOI 10.1002/pc

process usually took 2 min for 50–70°C drops in temperature. Then, tan(δ) values of the samples were measured by a time sweep experiment in order to study the micro-phase separation and hard domain aggregation at annealing temperature for 2 h. Then micro phase separated samples were heated from annealing temperature up to melting temperature. Schematic diagram of experiment is shown in Fig. 1.

RESULT AND DISCUSSION

Fourier Transform Infrared

FTIR was used to assess the effect of different parameters, i.e., shear, Closite30B, and MWCNTs, on micro-phase separation. Micro-phase separation was resulted from hydrogen bonding interactions between hard segments and was calculated using following formula based on the two absorption peaks located at 3,445 and 3,348/cm corresponding to the free and hydrogen-bonded *N—H* stretching, respectively,

$$DPS_{FTIR} = \frac{NH_{bonded}}{NH_{bonded} + NH_{free}} \quad (1)$$

From the results of this analysis, it can be concluded that MWCNTs in low content has the most important role in increasing phase separation. The high specific surface area of the carbon nanotube with low content provides effective surface for nucleation of hard segments, whereas, the higher content of nanoparticles reduces the phase separation due to inhibition of hard segment movements. Preshear increases hydrogen bonding interactions with arranging of hard segments, whereas, Closite30B has the negligible effect on phase separation [31]. The result can be observed in Fig. 2.

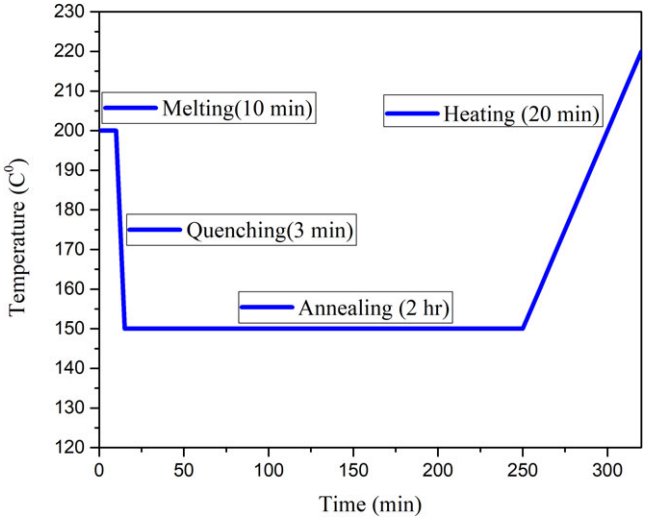

FIG. 1. Schematic diagram of rheological experiment. [Color figure can be viewed at wileyonlinelibrary.com]

Frequency Sweep

Frequency sweep diagrams of polyurethane nanocomposites with MWCNTs and Closite30B are represented in Fig. 3a, b. Closite30B has a very small aspect ratio and thus low interactions with polyurethane chains. It is evident that the almost all Closite30B loaded samples show terminal like behavior. Only the sample with high content of Closite30B (7%) revealed nonterminal behavior which can be assigned to formation of Closite30B clusters.

In MWCNTs loaded nanocomposites, because of high aspect ratio as well as high specific interactions with polymer chains, a nonterminal behavior was seen even at low content of MWCNTs. This occurrence can be assigned to interaction and confinement effects on carbon nanotubes on polyurethane chains. Whereas in nanoclay loaded samples with similar content of nanoparticle, nonterminal behavior has not been observed. To sum up, it can be perceived that carbon nanotubes made more interaction with polyurethane chains comparing clay nanoparticles [31–33].

Time Sweep Experiment

In this study, Tan (δ) is a criterion for investigation of phase separation of TPUs, because Tan (δ) shows ratio of storage modulus to loss modulus (Tan [δ] = $\frac{G''}{G'}$). When the sample is completely molten or phase separation is at beginning or phase separation has not occurred, loss modulus is bigger than storage modulus (Tan [δ] >1). When phase separation proceeds and hard domain agglomeration is formed, the sample possesses three-dimensional network and storage modulus becomes more than loss modulus (Tan [δ] <1). Some articles choose Tan (δ) =1 as a criterion when storage modulus crosses loss modulus. In this study, Tan (δ) of 0.8 has been used for a time of phase separation since when phase separation further proceeds Tan (δ) decreases and it is an easier indicator of phase separation.

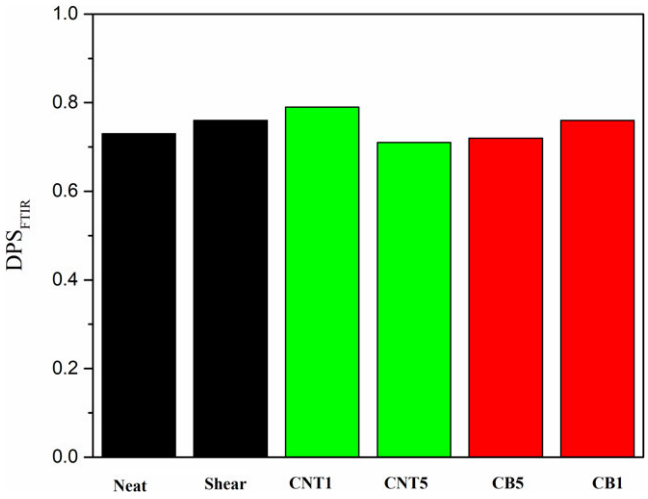

FIG. 2. Degree of phase separation of samples based on FTIR. [Color figure can be viewed at wileyonlinelibrary.com]

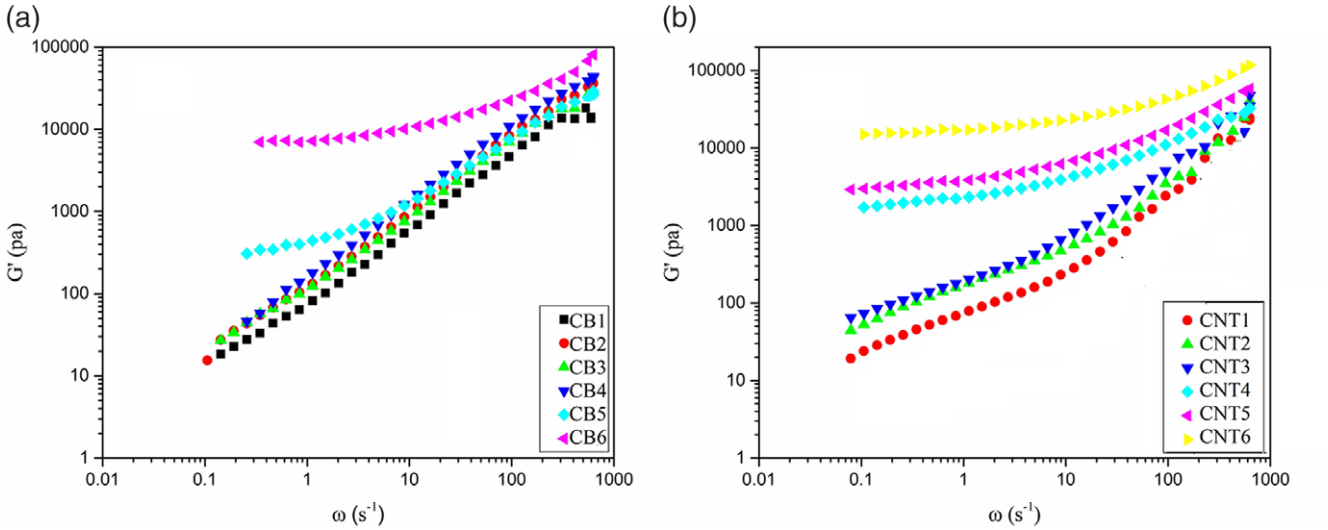

FIG. 3. Storage modulus of TPU nanocomposite (a) TPU/Closite30b (b) TPU/MWCNTs. [Color figure can be viewed at wileyonlinelibrary.com]

Time sweep diagrams of the samples are illustrated in Fig. 4. For this assay, at first the samples were heated at melting temperature for 10 min, then cooled to 150°C to phase separation occurred.

As it was mentioned earlier in this article, in the beginning that phase separation has not occurred, damp of samples was higher than 0.8. Because, the samples possessed viscous behavior and loss modulus was by far higher than storage modulus. Gradually, thermodynamic incompatibility between hard and soft segments occurred and hard domains were formed. Therefore, the storage modulus surpassed loss modulus and Tan (δ) became lower than 0.8.

Nanocomposite samples revealed lower value of Tan (δ) due to interaction of nanoparticles with polymer chains and decrement of chain dynamics. Among the nanocomposites, Tan (δ) of the sample with carbon nanotubes rapidly became 0.8 due to higher interaction and higher specific surface area of these particles for hard segment nucleation.

Moreover, presheared samples signified the higher initial damp. Because, preshear disturbed a few domains formed during cooling thus increasing Tan (δ) value. However, preshear accelerated phase separation due to orientation of chains and hard segments [6, 18].

Cooling Temperature Experiment

To evaluate the micro-phase separation temperature, time sweep cooling test was conducted. As it can be perceived from the previous analyses, presheared samples possess the highest damp. During cooling from T_m to T_g, at temperature that phase separation was started, the slope of storage modulus suddenly increased and Tan (δ) decreased

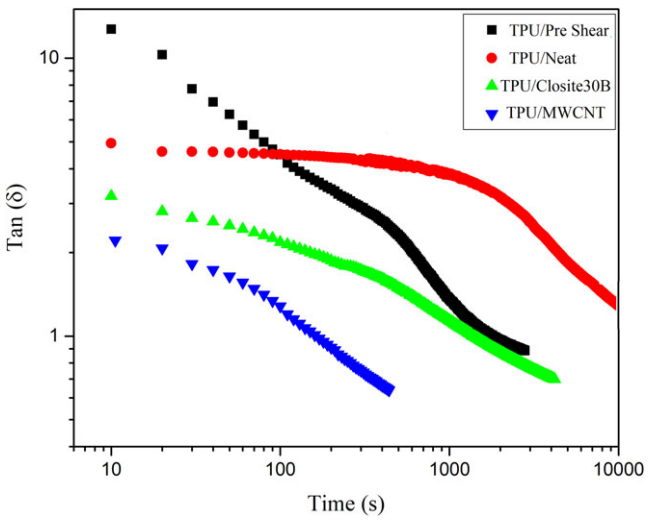

FIG. 4. Tan (δ) of samples as a function of time at 150°C. [Color figure can be viewed at wileyonlinelibrary.com]

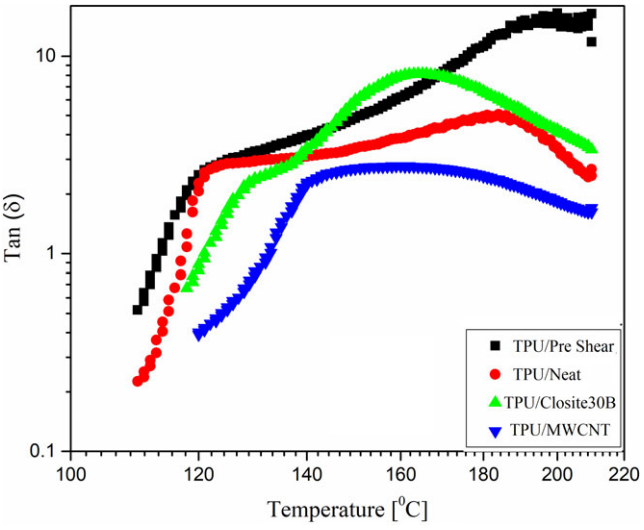

FIG. 5. Temperature sweep experiment with cooling rate 10°C/min. [Color figure can be viewed at wileyonlinelibrary.com]

DOI 10.1002/pc

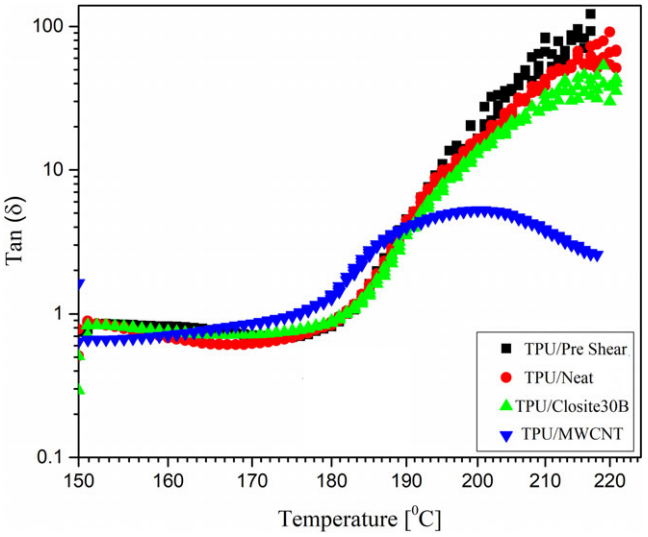

FIG. 6. Temperature sweep experiment with heating rate 10 °C/min. [Color figure can be viewed at wileyonlinelibrary.com]

to lower than one. This temperature can be an indicative of phase separation. As evidenced from the Fig. 5, presence of MWCNTs increased this temperature about 30°C comparing pristine polymer. Closite30B had no important influence on phase separation temperature [16, 31].

Heating Temperature Experiment

In heating analysis, all samples were firstly cooled to phase separation temperature, then were annealed for 2 h to ensure formation of domains and finally were heated. As time went by and phase separation occurred, Tan (δ) was definitely reduced to lower that 0.8. With increasing the temperature and destroying the hard domains, Tan (δ) was again increased to higher value (so much more than one). This temperature is ODT, the temperature in which the material changes from an ordered structure to a nonordered one. Due to higher nucleating effect of carbon nanotubes and their higher interaction with hard segments, more but smaller domains have been formed. These domains began to be melted at 167°C and increased Tan (δ) value to higher than 0.8. This phenomenon occurred for other samples at higher temperatures because their domains were larger. The exact temperatures are represented in Fig. 6 and Table 2 [34–36].

At the end of experimental section, the data are classified for neural network in Table 3. Where T is temperature (K), A_f is aspect ratio of nanofiller (A_f = 275 for MWCNTs and A_f = 10 for Closite30B) and φ is nanofiller percent.

Artificial Neural Network Model

Details of artificial neural network modeling using MLP are presented in literature [37–42]. ANN modeling can do the modeling without knowing the relationships between

TABLE 2. Transition temperature at time, cooling, and heating experiment RMS.

Sample	Temperature Tanδ = 0.8 cooling (°C)	Temperature Tanδ = 0.8 heating (°C)	Time of Tanδ = 0.8 time sweep(s)
Neat	118	155	12,500
Pre shear	113	162	2,640
Closite30B	120	156	3,700
MWCNTs	130	167	260

the variables or even the type of governing relationships between them. This great advantage of the neural network is very useful, especially when there is not enough information on relationships between variables or analytical formulation is time-consuming [43–47]. Probably the best type of feed forward network is the MLPs in which the information is transmitted only in forward direction between the layers. It generally consists of an input layer, an output layer, and one or more middle layers, which are referred to as hidden layers. The number of hidden layers depends on the complexity of the problem, the number of existing variables and relationships between them [48].

In each layer, there are a number of units called neurons. The number of neurons in the input layer is equal to the number of input variables, the number of neurons in the output layer is equal to the number of target variables and their number in the hidden layer(s) depends on the type of problem. One of the most influential issues in network performance is to find the suitable number of hidden layer neurons. In this study, There are three input neurons (temperature, nanoparticle's aspect ratio, and shear amount) and one output neuron (phase separation time). Figure 7 schematically shows the relationship between layers [49].

The task of neurons is to communicate between different layers. It should be noted that neurons do not interact with a specific layer. The input amount of each neuron for example *i*th neuron (s_i) is calculated using the formula below:

$$s_i = \sum_{j=1}^{n} \omega_{ij} y_j + B_i \tag{2}$$

Where *j*th neuron is located on the previous layer, ω_{ij}, B_i and y_j refer to the weight which is used to connect *i*th and *j*th neuron, bias related to neuron *i*th and input *j*th neuron, respectively, [50]. Transfer functions must be used to calculate the output of each neuron. Usually, between the hidden layer and the output layer, the pure linear transfer function is applied to achieve the best mapping. However, choosing the right transfer function between the input and hidden layer(s) is another factor that affects network performance. In this work, the nonlinear log-sigmoid transfer function showed better result than nonlinear tangent sigmoid transfer function.

To use the neural network, three steps must be taken. First, the data must be normalized, then the network should be trained, and the network should be tested at the end.

TABLE 3. Experimental data of time (min) Tanδ = 0.8 from time sweep.

Sample	T (K^0)	A_f*ϕ	Shear (s^{-1})	Time(min) Tanδ = 0.8
1	398	0	0	4.1
2	403	0	0	5.2
3	406	0	0	5.7
4	408	0	0	8.4
5	410	0	0	15.71
6	413	0	0	18.16
7	415.5	0	0	31.5
8	418	0	0	46.3
9	423	0	0	84
10	425	0	0	101.2
11	428	0	0	141.6
12	433	0	0	243.9
13	435.5	0	0	324.3
14	438	0	0	560.2
15	403	0	5	5.1
16	403	0	10	4.82
17	403	0	20	4.43
18	403	0	30	3.75
19	408	0	5	8.35
20	408	0	10	8.12
21	408	0	20	7.65
22	408	0	30	6.12
23	413	0	5	18
24	413	0	10	17.3
25	413	0	20	16.7
26	413	0	30	15.1
27	415.5	0	5	31.5
28	415.5	0	10	29.9
29	415.5	0	20	27.3
30	415.5	0	30	24.7
31	418	0	5	46.1
32	418	0	10	44
33	418	0	20	41.4
34	418	0	30	36.3
35	423	0	5	83.95
36	423	0	10	83.1
37	423	0	20	81.6
38	423	0	30	71.8
39	425	0	5	101
40	425	0	10	99.2
41	425	0	20	97.4
42	425	0	30	92.1
43	428	0	5	141.6
44	428	0	10	140
45	428	0	20	136.2
46	428	0	30	132.4
47	433	0	5	243.1
48	433	0	10	242.5
49	433	0	20	240.7
50	433	0	30	237.1
51	435.5	0	5	324.3
52	435.5	0	10	324
53	435.5	0	20	322.2
54	435.5	0	30	319.5
55	438	0	5	560.2
56	438	0	10	540.4
57	438	0	20	532.5
58	438	0	30	518.1
59	423	27.5	0	4.33
60	423	55	0	1.63
61	423	110	0	2.58
62	428	27.5	0	15.4

(Continues)

Table 3. Continued

Sample	T (K^0)	A_f*ϕ	Shear (s^{-1})	Time(min) Tanδ = 0.8
63	428	55	0	7.15
64	428	110	0	8.3
65	433	27.5	0	35.58
66	433	55	0	17.2
67	433	110	0	25.33
68	433	220	0	2.7
69	435.5	27.5	0	58.4
70	435.5	55	0	42.1
71	435.5	110	0	45.7
72	435.5	220	0	3.8
73	438	27.5	0	87.3
74	438	55	0	138.6
75	438	110	0	78.33
76	438	220	0	0.5
77	423	27.5	10	4.16
78	423	27.5	20	3.7
79	423	27.5	30	3.43
80	423	55	10	1.52
81	423	55	20	1.42
82	423	55	30	1.01
83	423	110	20	2.2
84	428	27.5	10	15.2
85	428	27.5	20	14.01
86	428	27.5	30	13
87	428	55	10	7.02
88	428	55	20	6.82
89	428	55	30	6.6
90	428	110	20	6.8
91	433	27.5	10	34.5
92	433	27.5	20	33.2
93	433	27.5	30	32.1
94	433	55	10	17.1
95	433	55	20	16.9
96	433	55	30	16.5
97	433	110	20	23.5
98	438	27.5	10	86.5
99	438	27.5	30	84.2
100	438	55	10	137.5
101	438	55	30	136.1
102	438	110	20	75.4
103	413	1	0	17.8
104	413	5	0	17.7
105	413	10	0	17.5
106	413	30	0	10.5
107	418	1	0	46.2
108	418	5	0	45.3
109	418	10	0	44.7
110	418	30	0	40.1
111	423	1	0	83.2
112	423	5	0	83
113	423	10	0	83.15
114	423	30	0	70.5
115	428	1	0	141
116	428	5	0	140.1
117	428	10	0	138.5
118	428	30	0	131.2
119	413	1	10	17.3
120	413	1	20	16.2
121	413	1	30	15.3
122	413	5	10	17.1
123	413	5	20	16
124	413	5	30	15.1

(Continues)

DOI 10.1002/pc

Table 3. Continued

Sample	T (K^0)	A_f*ϕ	Shear (s^{-1})	Time(min) Tanδ = 0.8
125	413	10	20	14.8
126	418	1	10	43.4
127	418	1	20	41.1
128	418	1	30	35.1
129	418	5	10	14.35
130	418	5	20	42.5
131	418	5	30	14
132	418	10	20	10.8
133	423	1	10	83
134	423	1	20	75.6
135	423	1	30	70.5
136	423	5	10	82.1
137	423	5	20	74.2
138	423	5	30	68
139	423	10	20	56.8
140	428	1	10	140.6
141	428	1	20	133.7
142	428	1	30	130.5
143	428	5	10	139.2
144	428	5	20	132.5
145	428	5	30	128.9
146	428	10	10	101.5
147	428	10	30	100.8
148	433	1	10	242.5
149	433	1	30	239.4
150	433	5	10	240
151	433	5	30	236.75
152	433	10	20	158.5

Therefore, the whole experimental data were normalized in the [0 1] range using *Eq. 3*:

$$X_{normal} = \frac{X_i - X_{min}}{X_{max} - X_{min}} \tag{3}$$

X_{max} and X_{min} refer to the minimum and maximum experimental data, respectively. In the next step, normalized data were randomly divided into two parts. The training set (106 sample) which represents 70% of the entire dataset is used to determine weights and bias. The predictive power of the model is tested by test data, which is 30% of the total experimental data (46 samples). During the training process, the neural network changes the weights and bias until the difference between the experimental data and the data produced by the model reach an acceptable difference. Back-propagation algorithm was used for network training because of its efficiency. Among the existing back-propagation algorithms, selecting the appropriate algorithm is important. In addition to reducing the gradient, the suitable algorithm has a high velocity and creates a good performance network. Criteria should be considered in order to compare with the performance of different algorithms. The criteria used in this study are mean square error (MSE), and coefficient of determination (R^2) [26]:

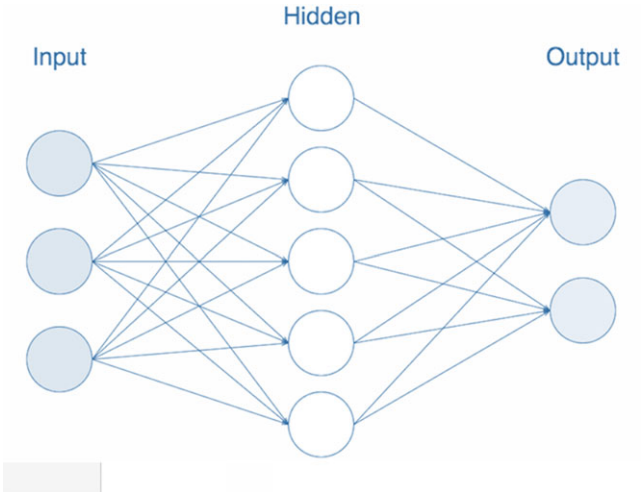

FIG. 7. A scheme of the neural network architecture. [Color figure can be viewed at wileyonlinelibrary.com]

$$MSE = \sum_{i=1}^{n} \left(Y_i^{exp} - Y_i^{ANN}\right)^2 \tag{4}$$

$$R^2 = \frac{\sum_{i=1}^{n} (Y_i^{exp} - \overline{Y})^2 - \sum_{i=1}^{n} (Y_i^{exp} - \overline{Yi^{ANN}})^2}{\sum_{i=1}^{n} (Y_i^{exp} - \overline{Y})^2} \tag{5}$$

Where n, Y^{exp}, Y^{ANN} are number of data, experimental data and estimated data, respectively. The bar sign represents the average value. The main point to be taken into consideration is that the network must not be over fitted.

Levenberg–Marquardt back propagation had the best performance in comparison with other algorithms, in addition to the proper speed, the accuracy was sufficient. The single hidden layer was selected to attain high stability and trouble-free training [51]. As previously mentioned, the number of hidden layer neurons is a very important parameter in determining the overall network behavior. Unfortunately, the correct way to find the number of hidden layer neurons has not been presented so far, and the only way to find the optimal number of neurons is the process of trial and error, which is very time-consuming [28, 52–54]. The optimal number of hidden neurons in this investigation is seven. Figure 8 shows optimal neural network architecture with three input variables, single hidden layer with seven neurons and one output variable. For the optimal network, the mean MSE is 33.16 and the R^2 is 0.99875.

Figure 9 Shows the linear regression of experimental data and data calculated by the ANN. As it is obvious in the figure, the calculated values are on the line 45°, which corroborates a very good match between the experimental data and the data obtained from the model. At the top of each Figure, the value of R is reported which is calculated from *Eq. 6*.

$$R = \frac{\sum_1^n (Y_{exp} - \overline{Y}_{exp})(Y_{ANN} - \overline{Y}_{ANN})}{\sqrt{\sum_1^n (Y_{exp} - \overline{Y}_{exp})^2 (Y_{ANN} - \overline{Y}_{ANN})^2}} \tag{6}$$

Figure 10 Shows amount of MSE in each iteration. It is seen that MSE values are reduced, whether for testing data

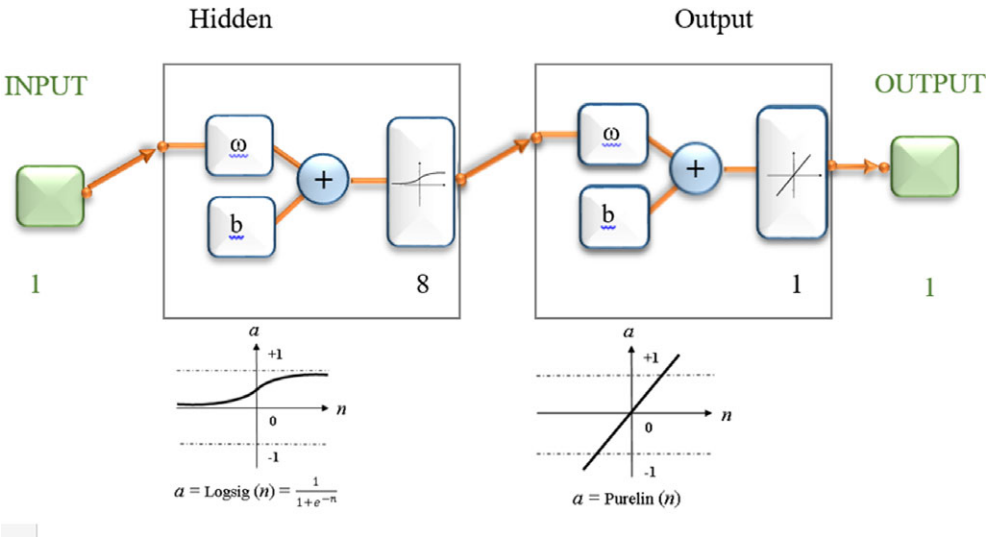

FIG. 8. Scheme of the optimal neural network architecture with three input variables (T, shear, Af*ϕ), single hidden layer with eight neurons and one target variable (phase separation time) with log-sig transfer function between input and hidden layer. [Color figure can be viewed at wileyonlinelibrary.com]

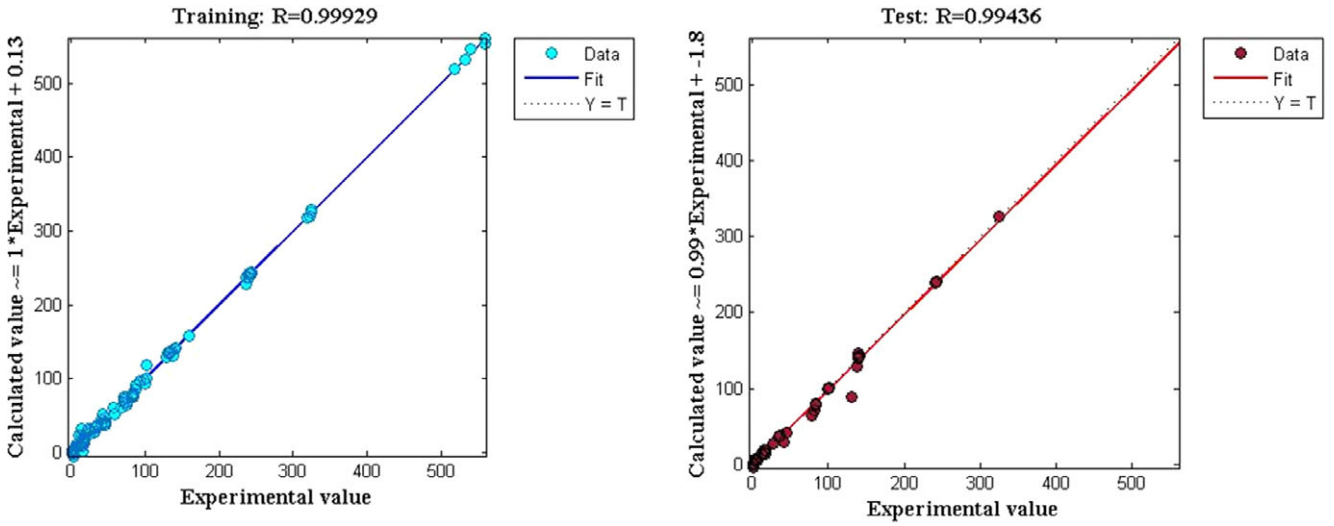

FIG. 9. Fitness plot for training and testing data set of ANN, the points show modeled data. [Color figure can be viewed at wileyonlinelibrary.com]

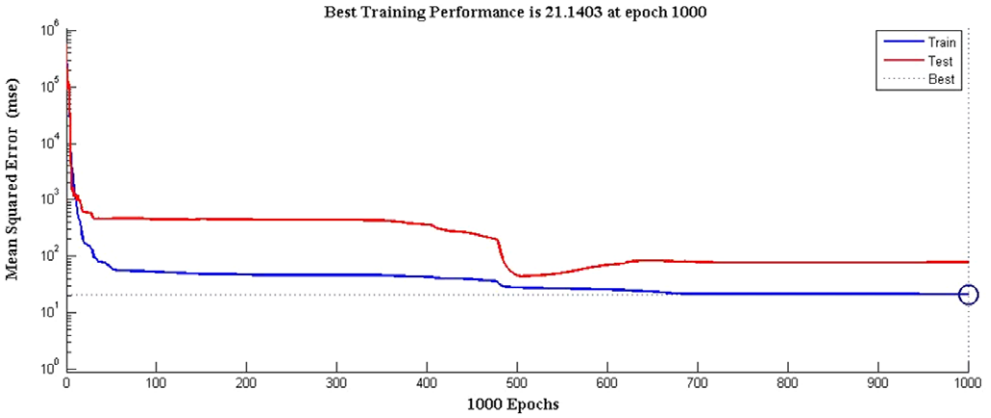

FIG. 10. Decreasing amount of MSE of training and test steps of network. [Color figure can be viewed at wileyonlinelibrary.com]

TABLE 4. Weight and biases of ANN for tan (δ).

Weight									Bias
ω_{ij}	1	2	3	4	5	6	7	8	B_i
Input layer—Hidden layer									
1	4.4964	18.7486	0.0359	—	—	—	—	—	6.8162
2	−0.8969	−21.0985	−0.1263	—	—	—	—	—	−18.0153
3	−32.5767	0.8129	43.6846	—	—	—	—	—	−2.3395
4	0.9906	−14.0279	−0.0014	—	—	—	—	—	−7.9733
5	−1.6763	1.5860	−0.0059	—	—	—	—	—	4.5163
6	0.5637	−11.2386	−0.0033	—	—	—	—	—	−6.3761
7	17.1988	−6.5825	−0.1123	—	—	—	—	—	−27.8715
8	−3.5108	−38.2371	−0.0621	—	—	—	—	—	−34.2123
Hidden layer—Output layer									
1	−3.1731	3.0781	0.0089	34.1169	−7.0278	−39.8554	34.4079	−0.7666	9.1317

or for training data. The final MSE values are close to each other indicating that the network behaves appropriately. By knowing the amount of weight and bias, the optimal network can be shared and used in new conditions. Therefore, the weight and bias values for the optimal design of the neural network are given in Table 4.

CONCLUSION

The neural network is able to predict micro-phase separation time of TPU nanocomposites possessing different nanofillers at various shear rates and temperatures. For modeling by ANN method, 80% of the experimental data were randomly selected for the neural network training process and the remaining 20% were used at the testing stage. After spending so much time, the neural network was obtained with a R^2_{total} of 0.99875 and MSE of 33.16. Comparison between experimental and calculated data by the model shows that the neural network can well communicate between input and target variables.

REFERENCE

1. J.O. Akindoyo, M.D.H. Beg, S. Ghazali, M.R. Islam, N. Jeyaratnam, and A.R. Yuvaraj, *RSC Adv.*, **6**(115), 114453 (2016).
2. M. Zajac, H. Kahl, B. Schade, T. Rodel, M. Dionisio, and M. Beiner, *Polymer (Guildf).*, **111**, 83 (2017).
3. A. Noreen, K.M. Zia, M. Zuber, S. Tabasum, and A. F. Zahoor, *Prog. Org. Coat.*, **91**, 25 (2016).
4. S. Velankar and S.L. Cooper, *Macromolecules*, **31**, 9181 (1998).
5. L.M. Leung and J.T. Koberstein, *Macromolecules*, **19**, 706 (1986).
6. C.D. Han, J. Kim, and J.K. Kim, *Macromolecules*, **22**, 383 (1989).
7. A. Rostami, M. Masoomi, M.J. Fayazi, and M. Vahdati, *RSC Adv.*, **5**(41), 32880 (2015).
8. A. Rostami, H. Nazockdast, and M. Karimi, *RSC Adv.*, **6**(55), 49747 (2016).
9. A. Shabani, A. Babaei, and A.R. Zanjanijam, *Polym. Adv. Technol.*, **2019**, 1 (2018).
10. S. Keshavarzi, A. Babaei, A. Goudarzi, and A. Shakeri, *Polym. Adv. Technol.*, **2019**, 1 (2018).
11. B. Finnigan, D. Martin, P. Halley, R. Truss, and K. Campbell, *J. Appl. Polym. Sci.*, **97**, 300 (2005).
12. M. Landa, J. Canales, M. Fernandez, M.E. Munoz, and A. Santamaria, *Polym. Test.*, **35**, 101 (2014).
13. A.K. Barick and A.K. Tripathy, *Mater. Sci. Eng.*, **176**, 1435 (2011).
14. Y.N. Gupta, T. Bhave, A. Chakraborty, A.K. Pandey, R.B. Sharma, and D.K. Setua, *Polym. Eng. Sci.*, **56**, 1248 (2018).
15. M. Song, H.S. Xia, K.J. Yao, and D.J. Hourston, *Eur. Polym. J.*, **41**, 259 (2005).
16. E. Mourier, L. David, P. Alcouffe, C. Rochas, and F. Méchin, *J. Polym. Sci. Part B Polym. Phys.*, **49**, 801 (2011).
17. E. Mourier, R. Fulchiron, and F. Mechin, *J. Polym. Sci. Part B Polym. Phys.*, **48**, 190 (2010).
18. A. Rostami, M. Vahdati, and H. Nazockdast, *Polym. Compos.*, **39**, 2356 (2018).
19. A. Rostami, M. Vahdati, Y. Alimoradi, M. Karimi, and H. Nazockdast, *Polymer (Guildf).*, **134**, 143 (2018).
20. A. Babaei and A. Arefazar, *J. Appl. Polym. Sci.*, **132**(20), 1 (2015).
21. Y. Ahmadzadeh, A. Babaei, and A. Goudarzi, *Polym. Degrad. Stab.*, **158**, 136 (2018).
22. L.B. Jack and A.K. Nandi, *Mech. Syst. Signal Process.*, **6**, 373 (2002).
23. D.H. Chang and S. Islam, *Remote Sens. Environ.*, **74**, 534 (2000).
24. S. Changyu, W. Lixia, and L. Qian, *J. Mater. Process. Technol.*, **183**, 412 (2007).
25. H. Hasnaoui, M. Krea, and D. Roizard, *J. Membr. Sci.*, **541**, 541 (2017).
26. M. Moghaddari, F. Yousefi, M. Ghaedi, and K. Dashtian, *Ultrason. Sonochem.*, **42**, 422 (2018).
27. F. Yousefi and H. Karimi, *Eur. Polym. J.*, **48**, 1135 (2012).
28. I. Kopal, M. Harničárová, and J. Valíček, *Polymer*, **9**, 1 (2017).
29. I. Sahebi Jouibari, V. Haddadi-Asl, and M.M. Mirhosseini, *Polym. Compos.*, **40**, E422 (2018).
30. X. Zhang, R. Xu, Z. Wu, and C. Zhou, *Polym. Int.*, **52**, 790 (2003).

31. I. Sahebi Jouibari, M. Kamkar, and H. Nazokdast, *Polym. Compos.*, **39**, 4551 (2018).
32. H. Koerner, J. Kelley, J. George, L. Drummy, P. Mirau, N. S. Bell, J.W.P. Hsu, and R.A. Vaia, *Macromolecules*, **42**, 8933 (2009).
33. J. Koberstein, I. Gancarz, and T.C. Clarke, *Polym. Phys.*, **24**, 2487 (1986).
34. F.S. Bates, J.H. Rosedale, and G.H. Fredrickson, *J. Chem. Phys.*, **92**, 6255 (1990).
35. M.D. Gehlsen, K. Almdal, and F.S. Bates, *Macromolecules*, **25**, 939 (1992).
36. C.D. Han, D.M. Baek, and J.K. Kim, *Macromolecules*, **23**, 561 (1990).
37. M. Aitkin and R. Foxall, *Stat. Comput.*, **13**, 227 (2003).
38. J. Boyd and H. White, *Conf. Neural Networks*, **4**, 2175 (1994).
39. B. Warner and M. Misra, *Am. Stat.*, **50**, 284 (1996).
40. D.F. Specht, *Neural Netw.*, **3**, 109 (1990).
41. W.B. Levy, *Int. Jt. Conf. Neural Networks*, 341 (1992).
42. T. Levin, N. Tishby, and S.A. Solla, *Proc. IEEE*, **78**, 1568 (1990).
43. T. Tchaban, J.P. Griffin, and J.M. Taylor, *Eng. Appl. Artif. Intell.*, **11**, 41 (1998).
44. K. Velten, R. Reinicke, and K. Friedrichrich, *Tribol. Int.*, **33**, 731 (2000).
45. N.K. Myshkin, O.K. Kwon, A.Y. Grigoriev, H.S. Ahn, and H. Kong, *Wear*, **203–204**, 658 (1997).
46. J.M. Schooling, M. Brown, and P.A.S. Reed, *Mater. Sci. Eng. A*, **260**, 222 (1999).
47. C. Dumortier and P. Lehert, *ISIJ Int.*, **39**, 980 (1999).
48. P. Assefi, M. Ghaedi, A. Ansari, M.H. Habibi, and M. S. Momeni, *J. Ind. Eng. Chem.*, **20**, 2905 (2014).
49. L.A. Gyurova and K. Friedrich, *Tribol. Int.*, **44**, 603 (2011).
50. K. Golzar, A. Jalali-Arani, and M. Nematollahi, *Constr. Build. Mater.*, **37**, 822 (2012).
51. J.S. Chang and B.C. Hung, *Ind. Eng. Chem. Res.*, **41**, 2716 (2002).
52. Y. Pan, J. Jiang, and Z. Wang, *J. Hazard. Mater.*, **147**, 424 (2007).
53. T. Puzyn and J. Falandysz, *J. Phys. Chem. Ref. Data*, **36**, 203 (2007).
54. W. Liu, P. Yi, and Z. Tang, *QSAR Comb. Sci.*, **25**, 936 (2007).